Efficient removal of Cu(II) and Pb(II) heavy metal ions from water samples using 2,4-dinitrophenylhydrazine loaded sodium dodecyl sulfate-coated magnetite nanoparticles

Soheil Sobhanardakani, Mazaher Ahmadi and Raziyeh Zandipak

ABSTRACT

This study reports on synthesis of a new nanoadsorbent for efficient Cu(II) and Pb(II) ions removal from water samples. In this regard, magnetite nanoparticles have been modified with 2,4-dinitrophenylhydrazine. The synthesized adsorbent has been fully characterized using scanning electron microscope, X-ray diffractometer, Fourier transform infrared spectrometer, and Brunauer, Emmett, and Teller measurements. The metal ions adsorption process has been thoroughly studied from both kinetic and equilibrium points of views. The adsorption isotherms were analyzed using five different isotherm models. It was found that the Sips isotherm showed better correlation with the experimental data than other isotherms, and the synthesized nanoadsorbent presents adsorption capacities for removal of Pb(II) and Cu(II) as high as 484.7 mg g^{-1} and 570.0 mg g^{-1}, respectively. The adsorption kinetics was tested for the pseudo-first order and pseudo-second order kinetic models at different experimental conditions. The kinetic data showed that the process is very fast and the adsorption process follows pseudo-second order kinetic models for modified magnetite adsorbents. The results suggest that the new nanoadsorbent is favorable and useful for the removal of the investigated metal ions under the optimized condition (pH: 6.0, adsorbent dosage: 0.02 g, agitation time: 45 min), and the high adsorption capacity makes it promising candidate material for metal ions removal from water samples.

Key words | 2,4-dinitrophenylhydrazine, flame atomic absorption spectrometry, heavy metal ions, magnetite nanoparticles, removal

Soheil Sobhanardakani (corresponding author)
Department of the Environment,
College of Basic Sciences,
Hamedan Branch,
Islamic Azad University,
Hamedan,
Iran
E-mail: *s_sobhan@iauh.ac.ir*

Mazaher Ahmadi
Raziyeh Zandipak
Young Researchers & Elite Club, Hamedan Branch,
Islamic Azad University,
Hamedan,
Iran

INTRODUCTION

Exposure to heavy metals, even at trace level, is believed to be a risk for human beings (Peng *et al.* 2004; Khan *et al.* 2008; Khani *et al.* 2010; Gupta *et al.* 2011; Hua *et al.* 2012). Thus, effective and deep removal of undesirable metals from water systems is a very important, but still challenging task for environmental engineers. Nowadays, numerous methods have been proposed for efficient heavy metal removal from waters, including but not limited to chemical precipitation, ion exchange, adsorption, membrane filtration, and electrochemical technologies (Wang *et al.* 2003; Afkhami *et al.* 2010; Fu & Wang 2011; Gupta *et al.* 2012a; Madrakian *et al.* 2012a, 2013a, 2015b). Among these techniques, adsorption offers flexibility in design and operation, and in many cases, it will generate high-quality treated effluent (Hua *et al.* 2012). Furthermore, owing to the reversible nature of most adsorption processes, the adsorbents can be regenerated by suitable desorption processes for multiple use (Ahmadi *et al.* 2015a; Madrakian *et al.* 2015b), and many desorption processes are of low maintenance cost, high efficiency, and ease of operation (Pan

doi: 10.2166/aqua.2016.100

et al. 2009). Therefore, the adsorption process has come to the forefront as one of the major techniques for heavy metal ions removal from water/wastewater samples.

Recently, application of nanoparticles for the removal of pollutants has arisen as an interesting area of research. The unique properties of nanosorbents are providing unprecedented opportunities for the removal of metals in highly efficient and cost-effective approaches, and various nanoparticles have been exploited for this purpose (Savage & Diallo 2005; Afkhami & Norooz-Asl 2009; Madrakian et al. 2011, 2013b, 2014b, 2015a, 2015b; Gupta et al. 2012b; Bagheri et al. 2015). Nanoparticles exhibit good adsorption efficiency especially due to higher surface area and greater active sites for interaction with metallic species. Furthermore, adsorbents with specific functional groups have been developed to improve the adsorption capacity (Afkhami et al. 2010). Among the available nanoadsorbents, nanosized metal oxides, including nanosized ferric oxides, manganese oxides, aluminum oxides, titanium oxides, magnesium oxides, and cerium oxides, are classified as the promising ones for heavy metals removal from aqueous systems (Agrawal & Sahu 2006; Afkhami et al. 2010; Madrakian et al. 2013a, 2014a).

Beside traditional nanosized metal oxides, magnetic nanoparticles such as iron oxides (Fe_3O_4 or γ-Fe_2O_3) have received much attention because of their interesting magnetic response, nanometer-scale properties, straightforward chemical modification, and excellent biocompatibility (Majewski & Thierry 2007; Reddy et al. 2012; Ahmadi et al. 2014; Bagheri et al. 2015). The magnetic separation provides a suitable route for online separation, where particles with affinity to target species are mixed with the solution. Upon mixing with the solution, the particles tag the target species. External magnetic fields are then applied to separate the tagged particles from the solution. Therefore, functionalized magnetic nanoparticles show great promise for applications in bioseparation (Pan et al. 2012), catalysis (Deng et al. 2010), drug delivery (Ruiz-Hernández et al. 2011; Ahmadi et al. 2015b), and magnetic resonance imaging (Lee & Hyeon 2012).

In the present work, 2,4-dinitrophenylhydrazine (DNPH) was immobilized on the surface of magnetite nanoparticles (MNPs) as a new nanoadsorbent for removing high levels of Pb(II) and Cu(II) from water samples. Experimental data, obtained from batch equilibrium tests, have been analyzed using different adsorption isotherm models (i.e., Langmuir, Freundlich, Sips, Redlich–Peterson, and Temkin isotherm models). The effects of various parameters, such as pH of the solutions, amount of adsorbent and contact time on the adsorption process were studied, and interpreted. In sum, this system has several advantages because the process does not generate secondary waste and the materials involved can be recycled and easily reused.

EXPERIMENTAL

Reagents and materials

All the chemicals used were of analytical reagent grade and were purchased from Merck Company (Darmstadt, Germany). Aqueous solutions of chemicals were prepared with deionized water (DI). All glassware was soaked in dilute nitric acid for 12 h, and then thoroughly rinsed with DI water. Standard solutions of Pb(II) and Cu(II) ions were prepared from the nitrates of these elements each as 1,000 mg L^{-1}. Working solutions, as per the experimental requirements, were freshly prepared from the stock solution for each experimental run. The adjustments of pH were performed with 0.01–1.0 mol L^{-1} HCl and/or NaOH solutions.

Apparatus

The concentration of the metal ions was determined by flame atomic absorption spectrometry (FAAS) using an Aurora model Spect AI 1200 apparatus. The instrumental settings of the manufacturer were followed. Infrared spectra were recorded with a Fourier transform infrared spectrometer (FT-IR) (Spectrum 100, Perkin Elmer). Samples were gently ground and diluted in KBr matrices to identify the functional groups and chemical bonding of the coated materials. The size, morphology, and structure of the nanoparticles were characterized by scanning electron microscope (SEM-EDX) (XL30, Philips, The Netherlands). Specific surface area and porosity were defined by N_2 adsorption–desorption porosimetry (77 K) using a porosimeter (Bel Japan, Inc.). The crystal structure of the synthesized materials was determined by an X-ray diffractometer (XRD) (38066 Riva, Italy) at

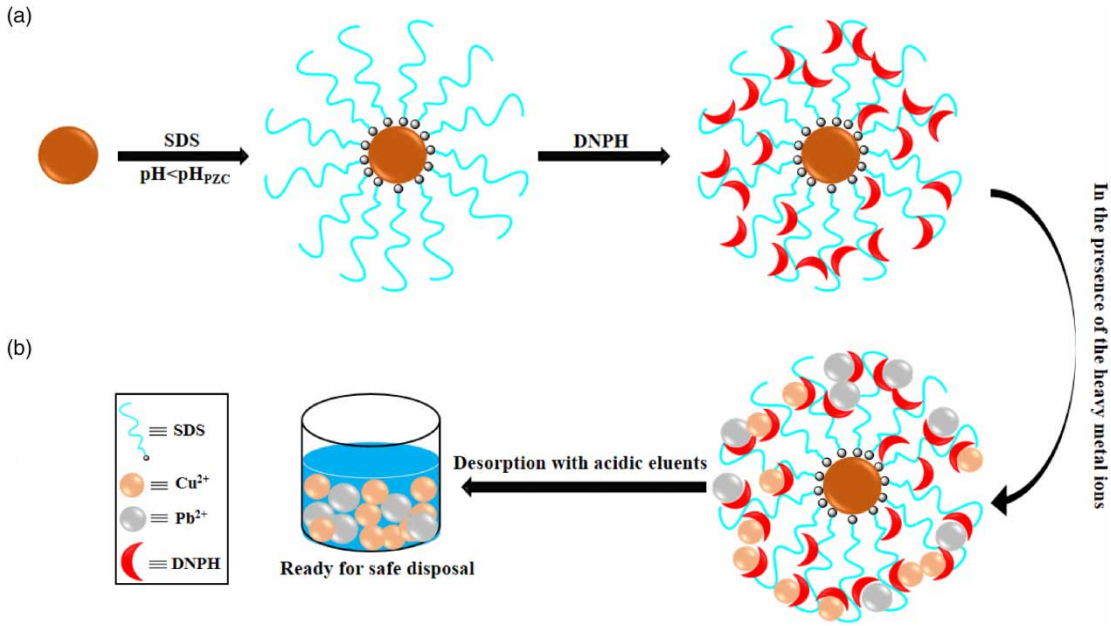

Figure 1 | Schematic diagram for (a) synthesis of the modified nanoparticles and (b) the heavy metal ions removal mechanism.

ambient temperature. A Metrohm model 713 (Herisau, Switzerland) pH-meter with a combined glass electrode was used for pH measurements.

Synthesis of MNPs, SDS coated magnetite nanoparticles, and DNPH modified SDS coated magnetite nanoparticles

The MNPs were prepared by the conventional co-precipitation method, with minor modifications (Madrakian *et al.* 2012b). 11.68 g of $FeCl_3{\cdot}6H_2O$ and 4.30 g of $FeCl_2{\cdot}4H_2O$ were dissolved in 200 mL DI water with vigorous stirring at 85 °C under nitrogen gas atmosphere. Then, 20 mL of 30% (w/v) aqueous NH_3 solution was added to the solution. The color of the bulk solution changed from orange to black immediately. The magnetite precipitates were washed twice with DI water and once with 0.02 mol L^{-1} sodium chloride by magnetic decantation.

Sodium dodecyl sulphate (SDS) coated magnetite nanoparticles (SDSMNPs) were prepared by adding 1.0 mL of 5% (w/v) SDS solution to 0.1 g of MNPs in a beaker at pH 3 (Figure 1(a)). The solution was stirred vigorously for 60 s by a glassy rod, and the beaker was then placed on the magnet. After complete precipitation of SDSMNPs, the solution was decanted and modified nanoparticles were washed with DI water four times to eliminate extra amounts of surfactant from the nanoparticles (Madrakian *et al.* 2013c). In order to prepare 2,4-dinitrophenylhydrazine modified SDS coated magnetite nanoparticles (DNPHMNPs), 20 mL of DNPH solution (0.01 mol L^{-1} in acetonitrile:acetic acid (2:1, v/v)) was added to the nanoparticles (SDSMNPs). Then, the suspension was stirred at 60 °C for 3 h. The mixture was followed by evaporation of the solvent, washing, air-drying, and storing in a closed bottle for subsequent use (Afkhami *et al.* 2010).

Adsorption studies

Adsorption studies (Figure 1(b)) were performed by adding 0.02 g DNPHMNPs to 20 mL solutions of different concentrations of the metal ions in a 50 mL beaker. The initial pH adjusted at 6.0 using 0.01–1.0 mol L^{-1} HCl and NaOH solutions. The quasi-equilibrium time was 45 min, when the adsorption behavior reached equilibrium. Then, the metal ions loaded nanoparticles were separated with magnetic decantation. The concentration of the metal ions in the solution was measured with FAAS. Concentration of the metal ions decreased with time due to adsorption by the modified nanoparticles. The adsorption percent, i.e., the metal ions

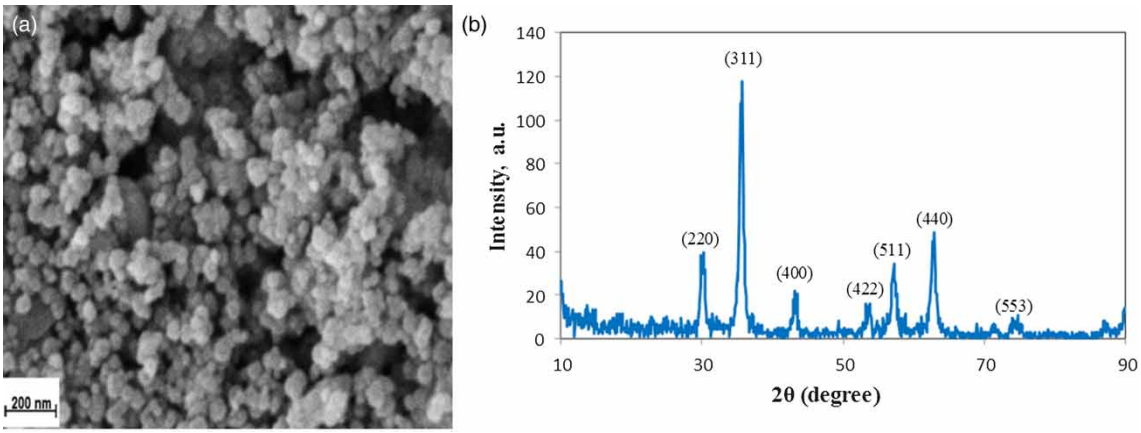

Figure 2 | SEM image (a) and XRD pattern (b) of the DNPHMNPs nanoparticles.

removal efficiency, was determined using the following expression:

$$\%Re = \left[\frac{(C_0 - C_t)}{C_0}\right] \times 100\% \quad (1)$$

where C_o and C_t represent the initial and final (after adsorption) concentration of the metal ions in mg L^{-1}, respectively.

Point of zero charge of the DNPHMNPs (pH_{PZC})

The point of zero charge (PZC) is a characteristic of metal oxides (hydroxides) and of fundamental importance in surface science. It is a concept relating to the phenomenon of adsorption and describes the condition when the electrical charge density on a surface is zero. In this study, the pH_{PZC} of the DNPHMNPs was determined using a previously reported method (Madrakian *et al.* 2013b). The pH_{PZC} for DNPHMNPs was determined using the above procedure and was obtained as almost 5.0 (results not shown).

RESULTS AND DISCUSSION

Characterization of the nanoadsorbent

The SEM image of the DNPHMNPs nanoparticles, as shown in Figure 2(a), revealed that the diameter of the modified nanoparticles was around 20–35 nm. The XRD pattern (Figure 2(b)) shows diffraction peaks that are indexed to (220), (311), (400), (422), (511), (440), and (553) reflection characteristics of the cubic spinel phase of Fe_3O_4 (JCPDS powder diffraction data file no. 79–0418), revealing that the resultant nanoparticles are mostly Fe_3O_4. The average crystallite size of the DNPHMNPs nanoparticles was estimated to be 15 nm from the XRD data according to the Scherrer equation (Madrakian *et al.* 2014a). As the results show, the particle dimension obtained by SEM is higher than the corresponding crystallite size. This difference may be explained because of the presence of aggregates in SEM grain consisting of several crystallites and/or poor crystallinity (Madrakian *et al.* 2013a).

The FT-IR spectra of DNPH, MNPs, and DNPHMNPs are shown in Figure 3. As shown in Figure 3(b), the peak at 580 cm^{-1} corresponds to Fe-O bond in Fe_3O_4. After modification of the magnetite with DNPH (Figure 3(c)), it shows a visible broad band in the 3,200–3,500 cm^{-1} region which is due to stretching vibrations of OH or N–H groups with varying degrees of hydrogen bonding. The absorption spectrum showed that the absorption bands at 1,345, 1,532, and 1,598 cm^{-1} are corresponding to the bending vibration of the N–H group (Figure 3(c)) (Afkhami *et al.* 2010; Madrakian *et al.* 2013c). Based on the above results, it can be concluded that the fabrication procedure has been successfully performed.

Specific surface areas are commonly reported as Brunauer, Emmett, and Teller (BET) surface areas obtained by applying the theory of BET to nitrogen adsorption/desorption isotherms measured at 77 K. The specific surface area of the sample was determined by physical adsorption of a gas on the surface of the solid by measuring the amount of adsorbed gas corresponding to a monomolecular layer on

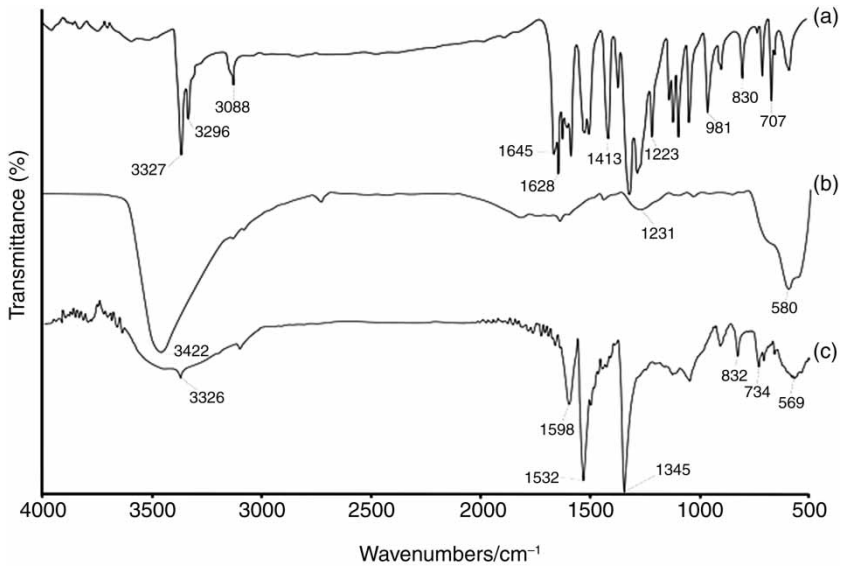

Figure 3 | The FT-IR spectra of (a) DNPH, (b) MNPs, and (c) DNPHMNPs.

the surface. The data are treated according to the BET theory (Brunauer *et al.* 1938). The results of the BET method showed that the average specific surface areas of the MNPs and DNPHMNPs nanoparticles were 99.3 m^2 g^{-1} and 75.5 m^2 g^{-1}, respectively. It can be concluded from these values that the synthesized nanoparticles have relatively large specific surface areas. This decrease in surface area of DNPHMNPs as compared to bare MNPs is possibly due to aggregation after the surface modification.

Effect of pH

One of the important factors affecting the removal of cations from aqueous solutions is the pH of the solution. The dependence of metal sorption on pH is related to both the metal chemistry in the solution and the ionization state of the functional groups of the sorbent, which affects the availability of binding sites. In order to evaluate the influence of this parameter on the adsorption of the metal cations, the experiments were carried out in the pH range of 3.0–9.0. A 0.03 g of the adsorbent was suspended in 20 mL solution of 20 mg L^{-1} of each of the metal ions at several pH values using either 0.1 M NaOH or 0.1 M HCl for the pH adjustment. These samples were stirred for 60 min. Then, the samples were magnetically filtered out. The results are shown in Figure 4.

As Figure 4 shows, the removal efficiencies of both the metal ions increase with increasing the solution pH, and a maximum value was reached at an equilibrium pH of around 6.0. A weak adsorption occurs in acid medium, but it can be seen that higher pH leads to higher metal uptake. Acidic conditions are not favorable because most of the functional groups of the adsorbent are protonated leaving few available ionized groups (Kwon *et al.* 2010). In addition, competition between protons and the metal species could explain the weak adsorption in acidic medium. The highest uptake value was recorded at the pH 6.0. This may be attributed to the presence of a free lone pair of electrons on

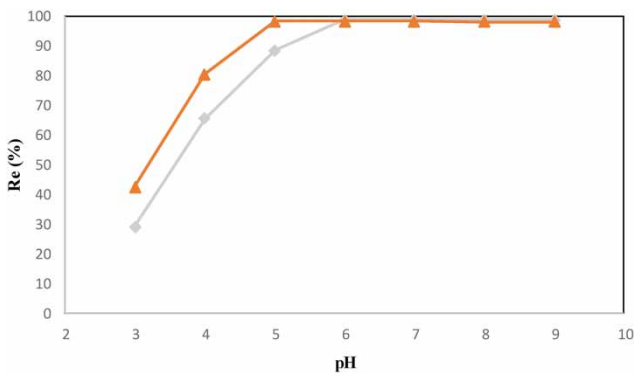

Figure 4 | Removal efficiencies of (▲) Cu(II) and (◆) Pb(II) at different pH values (conditions: 0.03 g of DNPHMNPs, 20 mL of 20.0 mg L^{-1} the metal ions, agitation time of 45 min).

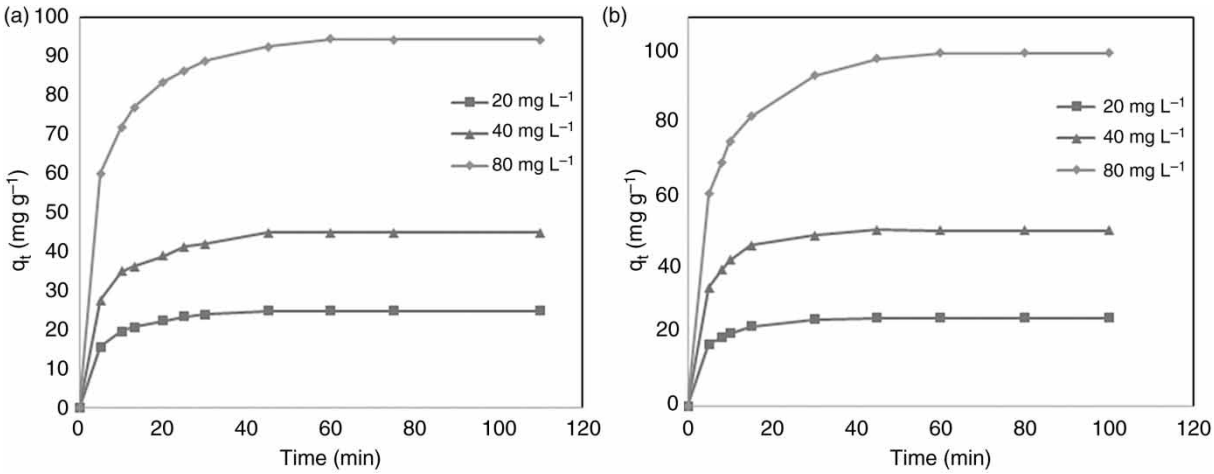

Figure 5 | Adsorption of (a) Cu(II) and (b) Pb(II) metal ions onto DNPHMNPs nanoparticles as a function of time at different initial concentration (conditions: pH 6, adsorbent dosage: 0.02 g, sample volume: 20 mL).

nitrogen and deprotonated hydroxyl group of the adsorbent (pH_{PZC} of DNPHMNPs: 5.0), which are suitable for coordination with the metal ions.

Effect of the adsorbent dosage

We studied the dependence of the adsorption of the cations on the amount of the modified nanoparticles at room temperature and at pH 6.0 by varying the adsorbent amount from 6 to 70 mg in contact with 20 mL solution of 20 mg L^{-1} of each cation. The suspension was then stirred for 60 min. After magnetically filtering, the supernatant was analyzed for the remaining cations. The results (not shown) showed that the percentage removal of the cations increased by increasing the amount of adsorbent due to the higher availability of the adsorbent. The adsorption reached a maximum with 0.02 g of adsorbent for both of the metal ions and the maximum percentage removal was about 99%.

Effect of agitation time

Figure 5 shows the effects of contact time on the adsorption of the metal ions at different initial concentrations. The metal ions reached equilibrium at about 45 min. In fact, 95% of the metal ions were adsorbed at about 30 min. To ensure the equilibrium, we used shaking for 45 min for all further experiments. The adsorption kinetics of the metal ions onto DNPHMNPs were investigated by pseudo-first order and pseudo-second order kinetic models, using Equations (2) and (3), respectively (Madrakian *et al.* 2015a).

Pseudo-first order model:

$$\ln(q_e - q_t) = lnq_e - k_1 t \tag{2}$$

Pseudo-second order model:

$$\frac{t}{q_t} = \frac{1}{k_2 q_e^2} + \frac{1}{q_e} t \tag{3}$$

where q_t (mg g^{-1}) is the adsorption capacity at time t (min); q_e (mg g^{-1}) is the adsorption capacity at adsorption equilibrium; and k_1 (min^{-1}) and k_2 (g mg^{-1} min^{-1}) are the kinetic rate constants for the pseudo-first order and the pseudo-second order models, respectively. The kinetic adsorption data were fitted to Equations (2) and (3), and the calculated results are shown in Table 1.

The best fit among the kinetic models is assessed by linear coefficient of determination (R^2), root-mean-square (RMS) error, and non-linear Chi-square (χ^2) test. The Chi-square test measures the difference between the experimental and model data. The mathematical form of this statistical test can be expressed as:

$$\chi^2 = \sum \frac{(q_{e,exp} - q_{e,cal})^2}{q_{e,cal}} \tag{4}$$

Table 1 | Adsorption kinetics model rate constant for the investigated metal ions adsorption onto the DNPHMNPs nanoparticles

Pseudo-second order						Pseudo-first order			
C_0 (mg L^{-1})	$q_{e,\ exp}$ (mg g^{-1})	$q_{e,\ cal}$ (mg g^{-1})	k_2 (g mg^{-1} min)	R^2	RMS	$q_{e,\ cal}$ (mg g^{-1})	k_1 (min^{-1})	R^2	RMS
Cu(II)									
20	24.81	25.11	0.011	0.9984	0.304	23.21	0.176	0.9884	0.834
40	44.97	44.22	0.005	0.9976	0.682	43.49	0.165	0.9800	1.978
80	94.50	96.55	0.002	0.9987	1.037	91.08	0.172	0.9798	4.140
Pb(II)									
20	24.98	24.65	0.015	0.9980	0.368	26.03	0.206	0.9896	0.829
40	49.81	52.16	0.007	0.9980	0.721	48.02	0.201	0.9945	1.200
80	99.87	97.64	0.002	0.9986	1.220	105.3	0.156	0.9860	3.876

where $q_{e,exp}$ is the experimental equilibrium capacity data and $q_{e,cal}$ is the equilibrium capacity from a model. If data from the model are similar to experimental data, χ^2 will be small, and if they differ, χ^2 will be large.

Fitted equilibrium adsorption capacities are similar at each initial concentration (for both the metal ions) and in close agreement with those observed experimentally. Furthermore, the correlation coefficients for the pseudo-second order kinetic model fits are much higher than the correlation coefficients derived from pseudo-first order model fits. Furthermore, the pseudo-second order kinetic model has lower RMS values than the other model. Given the good agreement between model fit and experimentally observed equilibrium adsorption capacity in addition to the large correlation coefficients and low RMS values, this suggests the complexation chemical reaction is expected in the adsorption processes (Zhou *et al.* 2009), and the rate-limiting step of the adsorption was dominated by a chemical adsorption process (Lin *et al.* 2011). The lower χ^2 values (Table 2) for the pseudo-second order model also suggests that the metal ions adsorption onto DNPHMNPs nanoparticles followed the pseudo-second order kinetics. The pseudo-first order model exhibited higher χ^2 values, suggesting poor pseudo-first order fit to the data for the metal ions adsorption onto DNPHMNPs.

Adsorption isotherms

The capacity of the adsorbent is an important factor that determines how much adsorbent is required for quantitative removal of a specific amount of the metal ions from solution. For measuring the adsorption capacity of the DNPHMNPs, the absorbent was added into the metal ions solutions at various concentrations (under the optimum condition as described above), and the suspensions were stirred at room temperature, followed by magnetic removal of the absorbent.

An adsorption isotherm describes the fraction of the sorbate molecules that are partitioned between the liquid and the solid phase at equilibrium. Adsorption of the metal ions by DNPHMNPs adsorbent was modeled using Freundlich (Freundlich & Heller 1939), Langmuir (Langmuir 1916), Redlich–Peterson (Redlich & Peterson 1959), Sips (Sips 1948), and Temkin (Temkin & Pyzhev 1940) adsorption isotherm models.

The linear form of the Langmuir isotherm is:

$$\frac{C_e}{q_e} = \frac{1}{K_L q_m} + \frac{1}{q_m} C_e \tag{5}$$

where K_L is a constant and C_e is the equilibrium concentration (mg L^{-1}); q_e is the amount of metal ion adsorbed per gram of adsorbent (mg g^{-1}) at equilibrium concentration C_e; and q_m is the maximum amount of solute adsorbed per

Table 2 | The χ^2 values for pseudo-first order and pseudo-second order models

Metal ions	Pseudo-second order	Pseudo-first order
Cu(II)	0.0598	0.2890
Pb(II)	0.1612	0.3890

gram of surface (mg g^{-1}), which depends on the number of adsorption sites. The Langmuir isotherm shows that the amount of solute adsorption increases as the concentration increases up to a saturation point.

The linear form of the Freundlich empirical model is represented by:

$$lnq_e = lnk_f + \frac{1}{n}C_e \tag{6}$$

where k_f ($mg^{1-1/n}\ L^{1/n}\ g^{-1}$) and $1/n$ are Freundlich constants depending on the temperature and the given adsorbent–adsorbate couple. The parameter 'n' is related to the adsorption energy distribution, and k_f indicates the adsorption capacity.

The Redlich–Peterson isotherm is an empirical isotherm incorporating three parameters. It combines elements from both the Langmuir and Freundlich equations, and the mechanism of adsorption is a hybrid, and does not follow ideal monolayer adsorption:

$$q_e = \frac{K_R C_e}{1 + \alpha_R C_e^{\beta}} \tag{7}$$

where K_R is the Redlich–Peterson isotherm constant (L g^{-1}); α_R is also a constant having unit of (mg^{-1}); and β is an exponent that lies between 0 and 1.

The Sips isotherm is a combined form of Langmuir and Freundlich expressions deduced for predicting the heterogeneous adsorption systems and circumventing the limitation of the rising adsorbate concentration associated with the Freundlich isotherm model. At low adsorbate concentrations, it reduces to the Freundlich isotherm, while at high concentrations, it predicts a monolayer adsorption capacity characteristic of the Langmuir isotherm:

$$q_e = \frac{q_m K_S C_e^{1/n}}{1 + K_S C_e^{1/n}} \tag{8}$$

where q_m is the Sips maximum adsorption capacity (mg g^{-1}); K_S is the Sips equilibrium constant (L mg^{-1}); and $1/n$ is the Sips model exponent.

The derivation of the Temkin isotherm assumes that the fall in the heat of adsorption is linear rather than logarithmic, as implied in the Freundlich equation. The linear form of the Temkin isotherm is:

$$q_e = \frac{RT}{b} lnK_T + \frac{RT}{b} lnC_e \tag{9}$$

where K_T is the equilibrium binding constant, corresponding to the maximum binding energy, and constant b is related to the heat of adsorption.

The remainder of the metal ions in the supernatants were measured by FAAS and the results were used to plot the isothermal adsorption curves as shown in Figure 6. The equilibrium adsorption data were fitted with the isotherm models with nonlinear regression, and the fitting parameter values are summarized in Table 3.

The higher values of R^2 and lower RMS values infer that the three parameter models best fit the adsorption equilibrium data and the best fitting isotherm model for both the metal ions is determined to be the Sips isotherm. The maximum adsorption capacities obtained from the Sips model for Pb(II) and Cu(II) are 484.7 mg g^{-1} and 570.0 mg g^{-1}, respectively. The different adsorption capacity may be due to disparity in cations' radius and interaction enthalpy values (Ge *et al.* 2012).

Desorption and reusability

In acidic solution the N donor of DNPH, which serves as an electron donor, can be protonated, resulting in a positive charge that repels the metal ions. Nevertheless, this can be

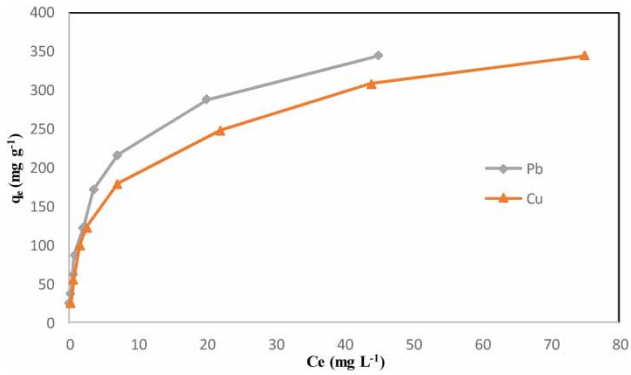

Figure 6 | Isotherm plots for adsorption of (▲) Cu(II) and (◆) Pb(II) metal ions onto the DNPHMNPs adsorbent.

Table 3 | Isotherm parameters for the two and three parameters adsorption isotherms for the adsorption of the metal ions onto DNPHMNPs at 298 K

Isotherm	Parameters	Pb(II)	Cu(II)
Langmuir			
	q_m (mg g^{-1})	349.68	369.15
	K_L(L mg^{-1})	0.288	0.157
	R^2	0.9738	0.9639
	RMS	19.56	26.68
Freundlich			
	K_F (L $mg^{(1-(1/n))}$/g)	101.60	87.11
	n	0.332	0.320
	R^2	0.9788	0.9833
	RMS	17.56	18.12
Temkin			
	B	37.01	59.14
	K_T (L mg^{-1})	42.30	3.99
	R^2	0.8000	0.9841
	RMS	54.02	16.65
Sips			
	q_m (mg g^{-1})	484.69	570.00
	K_S (L mg^{-1})	0.089	0.030
	n	1.648	1.853
	R^2	0.9943	0.9966
	RMS	8.77	8.75
Redlich–Peterson			
	K_R(L g^{-1})	228.45	167.0
	α_R (L mg^{-1})$^{1/\beta}$	1.383	1.214
	β	0.796	0.779
	R^2	0.9923	0.9913
	RMS	11.44	9.63

beneficial to the back-extraction step, because lowering solution pH facilitates decomplexation of the metal ions from the adsorbent. Desorption experiments were performed with different acidic eluents (0.05 M HCl, 0.05 M HNO_3 and a mixture of acetonitrile:0.05 M HNO_3 (1:1 v/v)). After adsorption of the metal ions, the adsorbent was magnetically separated. Then, 4.0 mL of the eluents was added to the separated adsorbent. Samples were collected after 5, 10, 20, and 30 min contact times with the eluent to evaluate the metal ions recovery by means of FAAS. Results showed that the mixture of acetonitrile:0.05 M HNO_3 (1:1 v/v) is the most effective back-extractant at desorption time of 10 min and could be used for the quantitative recovery of the metal ions.

The reusability and stability of DNPHMNPs for the removal of the metal ions were assessed by performing 20 consecutive separations/desorption cycles under the optimized conditions The results (Figure 7) showed that there was no significant change in the performance of the adsorbent during the first five cycles, indicating that the fabricated adsorbent is a reusable solid phase adsorbent for the removal of the metal ions during these five cycles. Furthermore, the results showed that the efficiencies of the recycled adsorbent for removing cations are nearly the same as those for the fresh ones even after recycling five times. Decrease in adsorption capacity in subsequent cycles may be due to the displacement of some adsorbed modifier molecules from SDSMNPs surface while treated with the eluent. Still, complete displacement of DNPH did not occur as considerable adsorption efficiency was observed in the next cycles. Reasonable removal efficiencies of the adsorbent in subsequent adsorption cycles made it a good choice for multi-cyclic usage.

In Table 4, the efficiency of the synthesized nanoparticles has been compared with some previously proposed adsorbents for removal of the investigated heavy metal ions. As can be seen, the synthesized nanoadsorbent has higher adsorption capacities in comparison to bare iron oxide nanoparticle (Grossl *et al.* 1994; Hu *et al.* 2006; Chen & Li 2010) and SDSMNPs (Adeli *et al.* 2012; Farahani & Shemirani 2014). It can be concluded that DNPH plays a critical role in improving the adsorbent efficiency. Furthermore, the adsorbent provides higher capacities in comparison to other metal oxides nanoparticles such as TiO_2 (Engates & Shipley 2011), ZnO (Ma *et al.* 2010), and CeO_2 (Cao *et al.* 2010). In addition, it can be seen that the used procedure to synthesize the adsorbent led to more

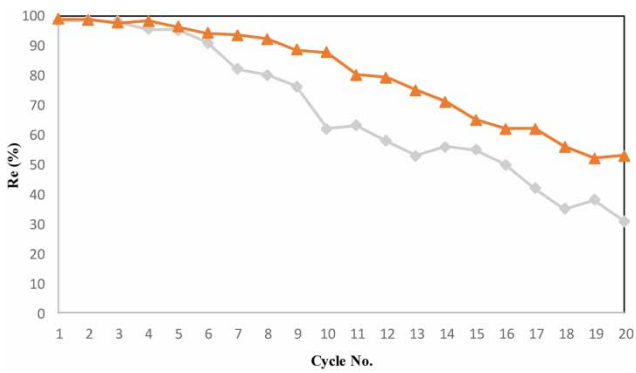

Figure 7 | The reusability and stability of DNPHMNPs for the removal of (▲) Cu(II) and (◆) Pb(II) (conditions: pH: 6.0, 0.02 g of DNPHMNPs, 20 mL of 20.0 mg L^{-1} the metal ions, agitation time of 45 min).

Table 4 | Comparison of the proposed method with some previously reported nanosized metal oxides for the metal ions removal

Adsorbent	Surface area ($m^2\ g^{-1}$)	Adsorption capacity ($mg\ g^{-1}$)		Isotherm model	Reference
		Cu(II)	Pb(II)		
Goethite (α-FeOOH)	50.0	149.25	–	–	Grossl *et al.* (1994)
Hematite (α-Fe_2O_3)	24.8	84.46	–	Langmuir	Chen & Li (2010)
Maghemite (γ-Fe_2O_3)	198.0	26.8	–	Langmuir	Hu *et al.* (2006)
SDS coated magnetite	–	24.3	–	Langmuir	Adeli *et al.* (2012)
SDS coated magnetite	–	–	9.5	–	Farahani & Shemirani (2014)
TiO_2	185.5	–	401.14	Langmuir	Engates & Shipley (2011)
DNPH modified γ-Al_2O_3	42.62	–	100*	Freundlich	Afkhami *et al.* (2010)
ZnO	–	–	6.7	—	Ma *et al.* (2010)
CeO_2	72	–	9.2	Langmuir	Cao *et al.* (2010)
p-nitro aniline modified magnetite (Fe_3O_4)	–	–	67.35	Langmuir	Madrakian *et al.* (2014b)
DNPH modified magnetite	75.5	570.00	484.69	Sips	This work

efficient nanoadsorbent in comparison to some other previously reported procedures with different nanoparticles (Afkhami *et al.* 2010) and ligands (Madrakian *et al.* 2014b).

CONCLUSION

In summary, the preparation and characterization of MNPs modified with DNPH for heavy metal ions removal purposes is described. The result shows that the synthesized nanoadsorbent is excellent for the removal of heavy metal ions such as Cu(II) and Pb(II) from aqueous solution. Furthermore, the adsorbent could efficiently remove the metal ions with higher adsorption capacities as compared with previously synthesized nanoadsorbents (Table 4) at pH 6.0, and could be used as a reusable adsorbent with convenient conditions. Moreover, considering reusability, easy synthesis, and separation, DNPHMNPs are superior to previously reported solid phase nanoadsorbents for heavy metal ions removal.

REFERENCES

Adeli, M., Yamini, Y. & Faraji, M. 2012 Removal of copper, nickel and zinc by sodium dodecyl sulphate coated magnetite nanoparticles from water and wastewater samples. *Arab. J. Chem.* DOI:10.1016/j.arabjc.2012.10.012.

Afkhami, A. & Norooz-Asl, R. 2009 Removal, preconcentration and determination of Mo(VI) from water and wastewater samples using maghemite nanoparticles. *Colloids Surf. A* **346**, 52–57.

Afkhami, A., Saber-Tehrani, M. & Bagheri, H. 2010 Simultaneous removal of heavy-metal ions in wastewater samples using nano-alumina modified with 2,4-dinitrophenylhydrazine. *J. Hazard. Mater.* **181**, 836–844.

Agrawal, A. & Sahu, K. K. 2006 Kinetic and isotherm studies of cadmium adsorption on manganese nodule residue. *J. Hazard. Mater.* **137**, 915–924.

Ahmadi, M., Madrakian, T. & Afkhami, A. 2014 Molecularly imprinted polymer coated magnetite nanoparticles as an efficient mefenamic acid resonance light scattering nanosensor. *Anal. Chim. Acta* **852**, 250–256.

Ahmadi, M., Madrakian, T. & Afkhami, A. 2015a Enantioselective solid phase extraction prior to spectrofluorometric determination: a procedure for the determination of naproxen enantiomers in the presence of each other. *RSC Adv.* **5**, 5450–5457.

Ahmadi, M., Madrakian, T. & Afkhami, A. 2015b Solid phase extraction of doxorubicin using molecularly imprinted polymer coated magnetite nanospheres prior to its spectrofluorometric determination. *New J. Chem.* **39**, 163–171.

Bagheri, H., Ahmadi, M., Madrakian, T. & Afkhami, A. 2015 Preconcentration and spectrofluorometric determination of L-tryptophan in the presence of D-tryptophan using a chiral magnetic nanoselector. *Sens. Actuat. B* **221**, 681–687.

Brunauer, S., Emmett, P. H. & Teller, E. 1938 Adsorption of gases in multimolecular layers. *J. Am. Chem. Soc.* **60**, 309–319.

Cao, C.-Y., Cui, Z.-M., Chen, C.-Q., Song, W.-G. & Cai, W. 2010 Ceria hollow nanospheres produced by a template-free microwave-assisted hydrothermal method for heavy

metal ion removal and catalysis. *J. Phys. Chem. C* **114**, 9865–9870.

Chen, Y.-H. & Li, F.-A. 2010 Kinetic study on removal of copper(II) using goethite and hematite nano-photocatalysts. *J. Colloid Interface Sci.* **347**, 277–281.

Deng, Y., Cai, Y., Sun, Z., Liu, J., Liu, C., Wei, J., Li, W., Liu, C., Wang, Y. & Zhao, D. 2010 Multifunctional mesoporous composite microspheres with well-designed nanostructure: a highly integrated catalyst system. *J. Am. Chem. Soc.* **132**, 8466–8473.

Engates, K. E. & Shipley, H. J. 2011 Adsorption of Pb, Cd, Cu, Zn, and Ni to titanium dioxide nanoparticles: effect of particle size, solid concentration, and exhaustion. *Environ. Sci. Pollt. Res. Int.* **18**, 386–395.

Farahani, M. D. & Shemirani, F. 2014 Mixed hemi-micelle solid-phase extraction based on modified magnetic nanoparticles for extraction of cadmium and lead from food and water samples. *J. AOAC Int.* **97**, 1682–1688.

Freundlich, H. & Heller, W. 1939 The adsorption of cis- and trans-azobenzene. *J. Am. Chem. Soc.* **61**, 2228–2230.

Fu, F. & Wang, Q. 2011 Removal of heavy metal ions from wastewaters: a review. *J. Environ. Manage.* **92**, 407–418.

Ge, F., Li, M. M., Ye, H. & Zhao, B. X. 2012 Effective removal of heavy metal ions Cd^{2+}, Zn^{2+}, Pb^{2+}, Cu^{2+} from aqueous solution by polymer-modified magnetic nanoparticles. *J. Hazard. Mater.* **211–212**, 366–372.

Grossl, P. R., Sparks, D. L. & Ainsworth, C. C. 1994 Rapid kinetics of Cu(II) adsorption/desorption on goethite. *Environ. Sci. Technol.* **28**, 1422–1429.

Gupta, V. K., Agarwal, S. & Saleh, T. A. 2011 Synthesis and characterization of alumina-coated carbon nanotubes and their application for lead removal. *J. Hazard. Mater.* **185**, 17–23.

Gupta, V. K., Ali, I., Saleh, T. A., Nayak, A. & Agarwal, S. 2012a Chemical treatment technologies for waste-water recycling – an overview. *RSC Adv.* **2**, 6380–6388.

Gupta, V. K., Jain, R., Mittal, A., Saleh, T. A., Nayak, A., Agarwal, S. & Sikarwar, S. 2012b Photo-catalytic degradation of toxic dye amaranth on TiO_2/UV in aqueous suspensions. *Mater. Sci. Eng. C* **32**, 12–17.

Hu, J., Chen, G. & Lo, I. 2006 Selective removal of heavy metals from industrial wastewater using maghemite nanoparticle: performance and mechanisms. *J. Environ. Eng.* **132**, 709–715.

Hua, M., Zhang, S., Pan, B., Zhang, W., Lv, L. & Zhang, Q. 2012 Heavy metal removal from water/wastewater by nanosized metal oxides: a review. *J. Hazard. Mater.* **211–212**, 317–331.

Khan, S., Cao, Q., Zheng, Y. M., Huang, Y. Z. & Zhu, Y. G. 2008 Health risks of heavy metals in contaminated soils and food crops irrigated with wastewater in Beijing, China. *Environ. Pollut.* **152**, 686–692.

Khani, H., Rofouei, M. K., Arab, P., Gupta, V. K. & Vafaei, Z. 2010 Multi-walled carbon nanotubes-ionic liquid-carbon paste electrode as a super selectivity sensor: application to potentiometric monitoring of mercury ion(II). *J. Hazard. Mater.* **183**, 402–409.

Kwon, J.-S., Yun, S.-T., Lee, J.-H., Kim, S.-O. & Jo, H. Y. 2010 Removal of divalent heavy metals (Cd, Cu, Pb, and Zn) and arsenic(III) from aqueous solutions using scoria: kinetics and equilibria of sorption. *J. Hazard. Mater.* **174**, 307–313.

Langmuir, I. 1916 The constitution and fundamental properties of solids and liquids. Part I. solids. *J. Am. Chem. Soc.* **38**, 2221–2295.

Lee, N. & Hyeon, T. 2012 Designed synthesis of uniformly sized iron oxide nanoparticles for efficient magnetic resonance imaging contrast agents. *Chem. Soc. Rev.* **41**, 2575–2589.

Lin, Y.-F., Chen, H.-W., Chien, P.-S., Chiou, C.-S. & Liu, C.-C. 2011 Application of bifunctional magnetic adsorbent to adsorb metal cations and anionic dyes in aqueous solution. *J. Hazard. Mater.* **185**, 1124–1130.

Ma, X., Wang, Y., Gao, M., Xu, H. & Li, G. 2010 A novel strategy to prepare ZnO/PbS heterostructured functional nanocomposite utilizing the surface adsorption property of ZnO nanosheets. *Catal. Today* **158**, 459–463.

Madrakian, T., Afkhami, A., Ahmadi, M. & Bagheri, H. 2011 Removal of some cationic dyes from aqueous solutions using magnetic-modified multi-walled carbon nanotubes. *J. Hazard. Mater.* **196**, 109–114.

Madrakian, T., Afkhami, A. & Ahmadi, M. 2012a Adsorption and kinetic studies of seven different organic dyes onto magnetite nanoparticles loaded tea waste and removal of them from wastewater samples. *Spectrochim. Acta A* **99**, 102–109.

Madrakian, T., Afkhami, A., Zolfigol, M. A., Ahmadi, M. & Koukabi, N. 2012b Application of modified silica coated magnetite nanoparticles for removal of iodine from water samples. *Nano-Micro Lett.* **4**, 57–63.

Madrakian, T., Afkhami, A. & Ahmadi, M. 2013a Simple in situ functionalizing magnetite nanoparticles by reactive blue-19 and their application to the effective removal of Pb^{2+} ions from water samples. *Chemosphere* **90**, 542–547.

Madrakian, T., Afkhami, A., Mahmood-Kashani, H. & Ahmadi, M. 2013b Superparamagnetic surface molecularly imprinted nanoparticles for sensitive solid-phase extraction of tramadol from urine samples. *Talanta* **105**, 255–261.

Madrakian, T., Afkhami, A., Rahimi, M., Ahmadi, M. & Soleimani, M. 2013c Preconcentration and spectrophotometric determination of oxymetholone in the presence of its main metabolite (mestanolone) using modified maghemite nanoparticles in urine sample. *Talanta* **115**, 468–473.

Madrakian, T., Afkhami, A., Haryani, R. & Ahmadi, M. 2014a Synthesis of γ-Fe_2O_3/TiO_2 nanocomposite and its application in removal of dyes from water samples by adsorption and degradation processes. *RSC Adv.* **4**, 44841–44847.

Madrakian, T., Afkhami, A., Rezvani-jalal, N. & Ahmadi, M. 2014b Removal and preconcentration of lead(II), cadmium(II) and chromium(III) ions from wastewater samples using surface functionalized magnetite nanoparticles. *J. Iran. Chem. Soc.* **11**, 489–498.

Madrakian, T., Afkhami, A., Zadpour, B. & Ahmadi, M. 2015a New synthetic mercaptoethylamino homopolymer-modified maghemite nanoparticles for effective removal of some heavy

metal ions from aqueous solution. *J. Indust. Eng. Chem.* **21**, 1160–1166.

Madrakian, T., Zadpour, B., Ahmadi, M. & Afkhami, A. 2015b Selective extraction and sensitive determination of mercury (II) ions by flame atomic absorption spectrometry after preconcentration on an ion-imprinted polymer-coated maghemite nanoparticles. *J. Iran. Chem. Soc.* **12**, 1235–1243.

Majewski, P. & Thierry, B. 2007 Functionalized magnetite nanoparticles – synthesis, properties, and bio-applications. *Crit. Rev. Solid State Mater. Sci.* **32**, 203–215.

Pan, B., Pan, B., Zhang, W., Lv, L., Zhang, Q. & Zheng, S. 2009 Development of polymeric and polymer-based hybrid adsorbents for pollutants removal from waters. *Chem. Eng. J.* **151**, 19–29.

Pan, Y., Du, X., Zhao, F. & Xu, B. 2012 Magnetic nanoparticles for the manipulation of proteins and cells. *Chem. Soc. Rev.* **41**, 2912–2942.

Peng, S. H., Wang, W. X., Li, X. & Yen, Y. F. 2004 Metal partitioning in river sediments measured by sequential extraction and biomimetic approaches. *Chemosphere* **57**, 839–851.

Reddy, L. H., Arias, J. L., Nicolas, J. & Couvreur, P. 2012 Magnetic nanoparticles: design and characterization, toxicity and biocompatibility, pharmaceutical and biomedical applications. *Chem. Rev.* **112**, 5818–5878.

Redlich, O. & Peterson, D. L. 1959 A useful adsorption isotherm. *J. Phys. Chem.* **63**, 1024.

Ruiz-Hernández, E., Baeza, A. & Vallet-Regí, M. 2011 Smart drug delivery through DNA/magnetic nanoparticle gates. *ACS Nano* **5**, 1259–1266.

Savage, N. & Diallo, M. 2005 Nanomaterials and water purification: opportunities and challenges. *J. Nanopart. Res.* **7**, 331–342.

Sips, R. 1948 On the structure of a catalyst surface. *J. Chem. Phys.* **16**, 490–495.

Temkin, M. & Pyzhev, V. 1940 Recent modifications to Langmuir isotherms. *Acta Phys. Chem.* **12**, 217–222.

Wang, Y.-H., Lin, S.-H. & Juang, R.-S. 2003 Removal of heavy metal ions from aqueous solutions using various low-cost adsorbents. *J. Hazard. Mater.* **102**, 291–302.

Zhou, Y.-T., Branford-White, C., Nie, H.-L. & Zhu, L.-M. 2009 Adsorption mechanism of Cu^{2+} from aqueous solution by chitosan-coated magnetic nanoparticles modified with α-ketoglutaric acid. *Colloids Surf. B* **74**, 244–252.

First received 28 August 2015; accepted in revised form 19 February 2016. Available online 21 March 2016